**EUROPEAN JOURNAL OF PURE AND APPLIED MATHEMATICS**
2025, Vol. 18, Issue 3, Article Number 6311
ISSN 1307-5543 – ejpam.com
Published by New York Business Global

# Fixed Point Techniques for Graph-Based Mappings with Image Recovery Approach

Sayan Panma[1,2], Raweerote Suparatulatorn[2,3], Tanadon Chaobankoh[1,2,*]

[1] *Department of Mathematics, Faculty of Science, Chiang Mai University, Chiang Mai 50200, Thailand*
[2] *Advanced Research Center for Computational Simulation, Chiang Mai University, Chiang Mai 50200, Thailand*
[3] *Department of Mathematics, Faculty of Science, Lampang Rajabhat University, Lampang 52100, Thailand*

**Abstract.** This article introduces an algorithm designed to approximate a common fixed point for a class of graph-based mappings in a real Hilbert space. We show that the sequence generated by this algorithm weakly converges to a common fixed point. Moreover, we explore the algorithm's practical application by investigating its effectiveness in solving image recovery problems related to fine particulate matter (PM2.5) pollution. Its performance is then evaluated by comparing it to existing methods.

**2020 Mathematics Subject Classifications**: 47J25, 47J26 65J15, 65Y05, 68W10

**Key Words and Phrases**: Fixed point problem, directed graph, G-nonexpansive mapping, image processing, process innovation

## 1. Introduction

The fixed point problem demonstrates exceptional versatility in addressing real-world challenges, particularly signal and image recovery. In this domain, iterative methods are used to extract solutions from noise-corrupted data. To enhance fixed point analysis, researchers have incorporated graph theory, as initially proposed by Jachymski [1]. By combining graph theory with mapping analysis, $G$-nonexpansive mappings represent a significant advancement in fixed point theory, contributing to the development of more powerful and efficient iterative schemes.

Recent studies have introduced algorithms for finding common fixed points of $G$-nonexpansive mappings in graph-based metric spaces. Khemphet et al. [2] improved signal

*Corresponding author.
DOI: https://doi.org/10.29020/nybg.ejpam.v18i3.6311

*Email addresses:* sayan.panma@cmu.ac.th (S. Panma),
raweerote.s@gmail.com (R. Suparatulatorn), tanadon.c@cmu.ac.th (T. Chaobankoh)

 

recovery using inertial and Mann iterations, demonstrating enhanced performance compared to previous methods. In a related work, Jun-On et al. [3] proposed a new inertial parallel algorithm for solving the common fixed point problem and applied it to signal recovery tasks. In 2024, a monotone hybrid algorithm based on a parallel inertial SP-iteration was proposed, with its weak convergence established and effectiveness demonstrated in solving linear systems, differential equations, and signal recovery problems [4]. Additionally, further research concerning this type of mappings can be found in, for example, the works of [5–9]. Through theoretical analysis and numerical experiments, these studies have collectively broadened the scope of fixed point theory for $G$-nonexpansive mappings.

With the growing urgency of environmental concerns, particularly fine particulate matter (PM2.5) pollution, methods are being developed to accurately estimate ground-level concentrations. In [10], an image-based PM2.5 estimation method using image processing and linear regression was proposed by analyzing differences between images with high and low PM2.5 concentrations. Also, in [11], the authors introduced a CNN-SVR approach for image-based PM2.5 estimation, enabling real-time analysis from single image captures. This approach, supported by its ability to handle extensive datasets and complex algorithms (see [12–14]) makes it a significant contribution to PM2.5 prediction, potentially improving air quality management.

In [15], an algorithm was presented for generating a sequence $\{x_n\}$ in a Banach space $E$, achieving faster convergence than Picard, Mann, and Agarwal et al. methods for nonexpansive mappings $T : E \to E$. The iterative process is given by:

$$\begin{cases} x_1 \in E, \\ x_{n+1} = (1-\alpha_n)Ty_n + \alpha_n Tz_n, \\ y_n = (1-\beta_n)Tx_n + \beta_n Tz_n, \\ z_n = (1-\gamma_n)x_n + \gamma_n Tx_n, \quad n \in \mathbb{N}, \end{cases} \tag{1}$$

where $\alpha_n, \beta_n, \gamma_n$ are sequences in the open unit interval.

Inspired by these findings, based on the iterative process (1), we develop Algorithm 1, a hybrid algorithm that combines the parallel monotone hybrid algorithm with the inertial method. We establish weak convergence theorems for finding common fixed points of $G$-nonexpansive mappings in real Hilbert spaces endowed with directed graphs $G$ under certain conditions. Finally, we validate our results through a real-world PM2.5-related image recovery task in Chiang Mai, Thailand, where we process images using multiple blurring filters and conduct a comparative analysis against existing algorithms presented in [3] and [4].

## 2. Preliminaries

In this section, we present some useful notations, definitions and results that will be used in the next section.

A directed graph $G$ consists of a non-empty vertex set $V(G)$ and an edge set $E(G)$, where each edge is an ordered pair that specifies a direction from one vertex to another.

A non-empty set $X$ is said to be equipped with a directed graph $G = (V(G), E(G))$ if $G$ has no parallel edges (i.e., all edges in $E(G)$ are distinct).

Throughout this article, we assume that $X := (X, \langle\cdot,\cdot\rangle)$ is a real Hilbert space, where $\|\cdot\|$ denotes the induced norm, and is equipped with a directed graph $G = (V(G), E(G))$. We also denote $\rightharpoonup$ and $\to$ as weak and strong convergence, respectively.

**Definition 1.** *[16] Let $J$ be a self-mapping on $X$. Then, $J$ is said to be G-nonexpansive if*

*(i) $J$ is edge-preserving, that is, for $u, v \in V(G)$,*

$$(u, v) \in E(G) \Rightarrow (Ju, Jv) \in E(G);$$

*(ii) for $u, v \in V(G)$,*

$$(u, v) \in E(G) \Rightarrow \|Ju - Jv\| \leq \|u - v\|.$$

**Definition 2.** *Let $J : X \to X$ be a self-mapping. A point $x \in X$ is called a fixed point of $J$ if*

$$J(x) = x.$$

*The set of fixed points of $J$, denoted $Fix(J)$, is defined as $\{x \in X : J(x) = x\}$.*

Let $\{J_1, J_2, \ldots, J_n\}$ be a collection of self-mappings on $X$. A point $x \in X$ is called a common fixed point of the mappings in this collection if it satisfies the condition:

$$J_i(x) = x \quad \text{for all } i = 1, 2, \ldots, n.$$

We list two essential facts in the following proposition. The first is a direct consequence of the definition of the squared norm and the properties of the inner product. The second, which is frequently used in the analysis of convex combinations, follows from the parallelogram law and can be found in [17].

**Proposition 1.** *For $x, y \in X$,*

$$\|x + y\|^2 \leq \|x\|^2 + 2\langle y, x + y\rangle, \text{ and} \tag{2}$$

$$\|\gamma x + (1 - \gamma)y\|^2 = \gamma\|x\|^2 + (1 - \gamma)\|y\|^2 - \gamma(1 - \gamma)\|x - y\|^2 \tag{3}$$

*for any $\gamma \in \mathbb{R}$.*

The following lemma provides a sufficient condition for the convergence of non-negative real number sequences and will be used in the next section.

**Lemma 1** ([18])**.** *Let $\{u_n\}$ and $\{v_n\}$ be sequences in $[0, \infty)$ such that $u_{n+1} \leq u_n + v_n$ for all $n$ and $\sum_{n=1}^{\infty} v_n < \infty$. Then, $\{u_n\}$ is a convergent sequence in $[0, \infty)$.*

## 3. Main results

Throughout this section, unless otherwise specified, we assume the following conditions hold.

(i) $E(G)$ is convex.

(ii) Each mapping $J_i : X \to X$ is $G$-nonexpansive for all $i = 1, 2, \ldots, N$.

(iii) $\mathrm{F} := \bigcap_{i=1}^{N} \mathrm{Fix}(J_i) \neq \emptyset$.

Building upon the preceding discussion, we now present our proposed algorithm inspired by the previous findings and based on the algorithm in [15], which combines the parallel monotone hybrid algorithm and the inertial method.

**Algorithm 1**

**Initialization:** Choose $x_0, x_1 \in X$, and let $n := 1$.
**Iterative Steps:** Iteratively construct the sequence $\{x_n\}$ as follows.
**Step 1.** Calculate

$$d_n = x_n + \beta_n(x_n - x_{n-1}),$$

where $\{\beta_n\}$ is a sequence of real numbers.
**Step 2.** Calculate

$$\begin{aligned} c_n^i &= (1 - \mu_n^i)d_n + \mu_n^i J_i d_n, \\ b_n^i &= (1 - \eta_n^i)J_i d_n + \eta_n^i J_i c_n^i, \end{aligned}$$

and

$$a_n^i = (1 - \sigma_n^i)J_i b_n^i + \sigma_n^i J_i c_n^i,$$

where $\{\mu_n^i\}, \{\eta_n^i\}$ and $\{\sigma_n^i\}$ are sequences in $[0, 1]$ for all $i = 1, 2, \ldots, N$.
**Step 3.** Set

$$x_{n+1} = \arg\max \left\{ \left\| a_n^i - d_n \right\| : i = 1, 2, \ldots, N \right\}.$$

Continue the iterative process by replacing $n$ with $n + 1$ and repeating all steps.

For convenience, we provide the following useful results, adapted to our current setting from [17] and [19], respectively.

**Observation 1.** *Let $\{x_n\}$ be a sequence in $X$ such that its weak sequential cluster points are in* F. *If $\{\|x_n - u\|\}$ is convergent for all $u \in$ F, then $\{x_n\}$ is weakly convergent in* F.

**Observation 2.** *For $i \in \{1, 2, 3, ..., N\}$, suppose that $\{u_n\}$ is a sequence in $X$ satisfying $u_n \rightharpoonup u$ and $(u_n - J_i u_n) \to 0$ for some $u \in X$. If there exists a subsequence $\{u_{n_k}\}$ of $\{u_n\}$ such that $(u_{n_k}, u) \in E(G)$ for all $k \in \mathbb{N}$, then $u \in \mathrm{F}$.*

We now let $\{x_n\}$ be a sequence generated by Algorithm 1. To facilitate the proof of our main result, we proceed by stating and proving the following lemmas.

**Lemma 2.** *Let $x^* \in \mathrm{F}$. Suppose that*

*(i)* $\sum_{n=1}^{\infty} |\beta_n| \|x_n - x_{n-1}\| < \infty$;

*(ii)* $\{(d_n, x^*), (x^*, d_n)\} \cap E(G) \neq \emptyset$.

*Then, $\{\|x_n - x^*\|\}$ is convergent and $\{x_n\}$ is bounded.*

*Proof.* From *(ii)*, we may assume that $(d_n, x^*) \in E(G)$. The edge-preserving property of $J_i$ implies that $(J_i d_n, x^*) = (J_i d_n, J_i x^*) \in E(G)$ for all $i = 1, 2, \ldots, N$. Then, it follows from the convexity of $E(G)$ that

$$(c_n^i, x^*) = ((1 - \mu_n^i) d_n + \mu_n^i J_i d_n, x^*) \in E(G).$$

Also, we obtain that $(J_i c_n^i, x^*)$, $(b_n^i, x^*)$, $(J_i b_n^i, x^*)$, and $(a_n^i, x^*) \in E(G)$ for all $i = 1, 2, \ldots, N$. Now, for any $i = 1, 2, \ldots, N$, from Proposition 1, we have the inequalities:

$$\begin{aligned}
\|J_i c_n^i - x^*\|^2 &\leq \|c_n^i - x^*\|^2 \\
&= \|(1 - \mu_n^i) d_n + \mu_n^i J_i d_n - x^*\|^2 \\
&= \|(1 - \mu_n^i)(d_n - x^*) + \mu_n^i (J_i d_n - x^*)\|^2 \\
&= (1 - \mu_n^i)\|d_n - x^*\|^2 + \mu_n^i \|J_i d_n - x^*\|^2 - (1 - \mu_n^i)\mu_n^i \|d_n - J_i d_n\|^2 \\
&\leq (1 - \mu_n^i)\|d_n - x^*\|^2 + \mu_n^i \|d_n - x^*\|^2 - (1 - \mu_n^i)\mu_n^i \|d_n - J_i d_n\|^2 \\
&= \|d_n - x^*\|^2 - (1 - \mu_n^i)\mu_n^i \|d_n - J_i d_n\|^2,
\end{aligned}$$

and

$$\begin{aligned}
\|J_i b_n^i - x^*\|^2 &\leq \|b_n^i - x^*\|^2 \\
&\leq (1 - \eta_n^i)\|J_i d_n - x^*\|^2 + \eta_n^i \|J_i c_n^i - x^*\|^2 \\
&\leq (1 - \eta_n^i)\|d_n - x^*\|^2 + \eta_n^i \|d_n - x^*\|^2 - \eta_n^i (1 - \mu_n^i)\mu_n^i \|d_n - J_i d_n\|^2 \\
&= \|d_n - x^*\|^2 - \eta_n^i (1 - \mu_n^i)\mu_n^i \|d_n - J_i d_n\|^2. \qquad (4)
\end{aligned}$$

Consequently, we have the following.

$$\begin{aligned}
\|a_n^i - x^*\|^2 &\leq (1 - \sigma_n^i)\|J_i b_n^i - x^*\|^2 + \sigma_n^i \|J_i c_n^i - x^*\|^2 \\
&\leq (1 - \sigma_n^i)\|d_n - x^*\|^2 - (1 - \sigma_n^i)\eta_n^i (1 - \mu_n^i)\mu_n^i \|d_n - J_i d_n\|^2 \\
&\quad + \sigma_n^i \|d_n - x^*\|^2 - \sigma_n^i (1 - \mu_n^i)\mu_n^i \|d_n - J_i d_n\|^2
\end{aligned}$$

$$= \|d_n - x^*\|^2 - (1-\sigma_n^i)\eta_n^i(1-\mu_n^i)\mu_n^i\|d_n - J_i d_n\|^2 - \sigma_n^i(1-\mu_n^i)\mu_n^i\|d_n - J_i d_n\|^2. \tag{5}$$

This implies that

$$\begin{aligned}\|a_n^i - x^*\| &\leq \|d_n - x^*\| \\ &= \|x_n + \beta_n(x_n - x_{n-1}) - x^*\| \\ &\leq \|x_n - x^*\| + |\beta_n|\|x_n - x_{n-1}\|.\end{aligned}$$

Finally, we obtain that

$$\|x_{n+1} - x^*\| \leq \|x_n - x^*\| + |\beta_n|\|x_n - x_{n-1}\|.$$

By $(i)$ and Lemma 1, the sequence $\{\|x_n - x^*\|\}$ is convergent and thus $\{x_n\}$ is bounded.

**Lemma 3.** *Assume that for all $i = 1, 2, \ldots, N$, the following conditions are met:*

*(i)* $\sum_{n=1}^{\infty} |\beta_n|\|x_n - x_{n-1}\| < \infty$;

*(ii)* $(d_n, x^*), (x^*, d_n) \in E(G)$ *for all* $x^* \in \mathrm{F}$;

*(iii)* $0 < \liminf_{n\to\infty} \mu_n^i \leq \limsup_{n\to\infty} \mu_n^i < 1$;

*(iv)* $\liminf_{n\to\infty} \sigma_n^i > 0$;

*(v) $G$ is transitive.*

*Then,* $\lim_{n\to\infty} \|d_n - J_i d_n\| = 0$ *for all* $i = 1, 2, \ldots, N$.

*Proof.* Let $x^* \in \mathrm{F}$. We first consider the following calculations.
From inequalities (2) and (5), and the definition of $\{d_n\}$,

$$\begin{aligned}\|a_n^i - x^*\|^2 &\leq \|x_n - x^* + \beta_n(x_n - x_{n-1})\|^2 \\ &\quad - (1-\sigma_n^i)\eta_n^i(1-\mu_n^i)\mu_n^i\|d_n - J_i d_n\|^2 - \sigma_n^i(1-\mu_n^i)\mu_n^i\|d_n - J_i d_n\|^2 \\ &\leq \|x_n - x^*\|^2 + 2\langle\beta_n(x_n - x_{n-1}), d_n - x^*\rangle \\ &\quad - (1-\sigma_n^i)\eta_n^i(1-\mu_n^i)\mu_n^i\|d_n - J_i d_n\|^2 - \sigma_n^i(1-\mu_n^i)\mu_n^i\|d_n - J_i d_n\|^2 \\ &\leq \|x_n - x^*\|^2 + 2|\beta_n|\|x_n - x_{n-1}\|\|d_n - x^*\| \\ &\quad - (1-\sigma_n^i)\eta_n^i(1-\mu_n^i)\mu_n^i\|d_n - J_i d_n\|^2 - \sigma_n^i(1-\mu_n^i)\mu_n^i\|d_n - J_i d_n\|^2. \end{aligned} \tag{6}$$

From (6), there exists some $i_n$ such that $x_{n+1} = a_n^{i_n}$ and that

$$\sigma_n^{i_n}(1-\mu_n^{i_n})\mu_n^{i_n}\|d_n - J_{i_n} d_n\|^2 \leq \|x_n - x^*\|^2 - \|x_{n+1} - x^*\|^2 + 2|\beta_n|\|x_n - x_{n-1}\|\|d_n - x^*\|.$$

It is clear that the right handed side of (6) tends to zero when $n \to \infty$. Therefore

$$\lim_{n\to\infty} \|d_n - J_{i_n} d_n\| = 0. \tag{7}$$

Next, we will show that $\lim_{n\to\infty} \|d_n - J_i d_n\| = 0$. By the triangle inequality and the $G$-nonexpansivity of $J_{i_n}$, we have that

$$\begin{aligned}
\|x_{n+1} - d_n\| &\leq (1-\sigma_n^{i_n})\|J_{i_n} b_n^{i_n} - d_n\| + \sigma_n^{i_n}\|J_{i_n} c_n^{i_n} - d_n\| \\
&\leq (1-\sigma_n^{i_n})\|J_{i_n} b_n^{i_n} - J_{i_n} d_n\| + (1-\sigma_n^{i_n})\|J_{i_n} d_n - d_n\| \\
&\quad + \sigma_n^{i_n}\|J_{i_n} c_n^{i_n} - J_{i_n} d_n\| + \sigma_n^{i_n}\|J_{i_n} d_n - d_n\| \\
&\leq (1-\sigma_n^{i_n})\|b_n^{i_n} - d_n\| + \|J_{i_n} d_n - d_n\| + \sigma_n^{i_n}\|J_{i_n} c_n^{i_n} - J_{i_n} d_n\| \\
&\leq (1-\sigma_n^{i_n})\|b_n^{i_n} - J_{i_n} d_n\| + (2-\sigma_n^{i_n})\|J_{i_n} d_n - d_n\| + \sigma_n^{i_n}\|J_{i_n} c_n^{i_n} - J_{i_n} d_n\|.
\end{aligned}$$

We obtain the following calculations by applying the definitions of $b_n^{i_n}$ and $c_n^{i_n}$ together with the $G$-nonexpansivity of $J_{i_n}$:

$$\begin{aligned}
\|x_{n+1} - d_n\| &\leq (1-\sigma_n^{i_n})\eta_n^{i_n}\|J_{i_n} c_n^{i_n} - J_{i_n} d_n\| + (2-\sigma_n^{i_n})\|J_{i_n} d_n - d_n\| + \sigma_n^{i_n}\|J_{i_n} c_n^{i_n} - J_{i_n} d_n\| \\
&= \{(1-\sigma_n^{i_n})\eta_n^{i_n} + \sigma_n^{i_n}\}\|J_{i_n} c_n^{i_n} - J_{i_n} d_n\| + (2-\sigma_n^{i_n})\|J_{i_n} d_n - d_n\| \\
&\leq \{(1-\sigma_n^{i_n})\eta_n^{i_n} + \sigma_n^{i_n}\}\|c_n^{i_n} - d_n\| + (2-\sigma_n^{i_n})\|J_{i_n} d_n - d_n\| \\
&= \{(1-\sigma_n^{i_n})\eta_n^{i_n} + \sigma_n^{i_n}\}\mu_n^{i_n}\|J_{i_n} d_n - d_n\| + (2-\sigma_n^{i_n})\|J_{i_n} d_n - d_n\| \\
&= [\{(1-\sigma_n^{i_n})\eta_n^{i_n} + \sigma_n^{i_n}\}\mu_n^{i_n} + (2-\sigma_n^{i_n})]\|J_{i_n} d_n - d_n\|.
\end{aligned} \tag{8}$$

By (7), taking $n \to \infty$, we can conclude that

$$\lim_{n\to\infty} \|a_n^i - d_n\| = 0 \text{ for all } i = 1, 2, \ldots, N.$$

Now, it follows from (5) that there exists a constant $C > 0$ such that

$$\begin{aligned}
\sigma_n^i(1-\mu_n^i)\mu_n^i\|d_n - J_i d_n\|^2 &\leq \|d_n - x^*\|^2 - \|a_n^i - x^*\|^2 \\
&\quad - (1-\sigma_n^i)\eta_n^i(1-\mu_n^i)\mu_n^i\|d_n - J_i d_n\|^2 \\
&\leq C(\|d_n - x^*\| - \|a_n^i - x^*\|) \\
&\leq C\|d_n - a_n^i\|.
\end{aligned}$$

Finally, we have that

$$\lim_{n\to\infty} \|d_n - J_i d_n\| = 0$$

for all $i = 1, 2, \ldots, N$.

Analogously, we establish the following lemma using a similar approach.

**Lemma 4.** *Assume that for all $i = 1, 2, \ldots, N$, the following conditions are met:*

*(i)* $\sum_{n=1}^{\infty} |\beta_n| \|x_n - x_{n-1}\| < \infty$;

*(ii)* $(d_n, x^*), (c_n^i, d_n)$ *and* $(b_n^i, d_n) \in E(G)$ *for all* $x^* \in \mathrm{F}$;

*(iii)* $0 < \liminf_{n\to\infty} \mu_n^i \leq \limsup_{n\to\infty} \mu_n^i < 1$;

*(iv)* $\liminf_{n\to\infty} \sigma_n^i > 0$.

*Then,* $\lim_{n\to\infty} \|d_n - J_i d_n\| = 0$ *for all* $i = 1, 2, \ldots, N$.

*Proof.* Here, we replace conditions (ii) and (iv) of Lemma 3 with condition (ii) of Lemma 4. The proof then proceeds similarly to that of Lemma 3.

Subsequently, after replacing certain assumptions, we present the following lemma.

**Lemma 5.** *Assume that for all* $i = 1, 2, \ldots, N$, *the following conditions are met:*

*(i)* $\sum_{n=1}^{\infty} |\beta_n| \|x_n - x_{n-1}\| < \infty$;

*(ii)* $(d_n, x^*), (x^*, d_n) \in E(G)$ *for all* $x^* \in \mathrm{F}$;

*(iii)* $0 < \liminf_{n\to\infty} \mu_n^i \leq \limsup_{n\to\infty} \mu_n^i < 1$;

*(iv)* $\liminf_{n\to\infty} \eta_n^i > 0$ *and* $\limsup_{n\to\infty} \sigma_n^i < 1$;

*(v) G is transitive.*

*Then,* $\lim_{n\to\infty} \|d_n - J_i d_n\| = 0$ *for all* $i = 1, 2, \ldots, N$.

*Proof.* Let $x^* \in \mathrm{F}$. It follows from (6) that

$$\|a_n^i - x^*\|^2 \leq \|x_n - x^*\|^2 + 2|\beta_n| \|x_n - x_{n-1}\| \|d_n - x^*\| - (1 - \sigma_n^i)\eta_n^i(1 - \mu_n^i)\mu_n^i \|d_n - J_i d_n\|^2.$$

Based on this, we observe that

$$(1 - \sigma_n^{i_n})\eta_n^{i_n}(1 - \mu_n^{i_n})\mu_n^{i_n} \|d_n - J_{i_n} d_n\|^2 \leq \|x_n - x^*\|^2 - \|x_{n+1} - x^*\|^2 + 2|\beta_n| \|x_n - x_{n-1}\| \|d_n - x^*\|.$$

This leads to the conclusion that

$$\lim_{n\to\infty} \|d_n - J_{i_n} d_n\| = 0.$$

Next, by (8), we have that

$$\|x_{n+1} - d_n\| \leq \left(\{(1 - \sigma_n^{i_n})\eta_n^{i_n} + \sigma_n^{i_n}\}\mu_n^{i_n} + (2 - \sigma_n^{i_n})\right) \|J_{i_n} d_n - d_n\|.$$

Accordingly,

$$\lim_{n\to\infty} \|a_n^i - d_n\| = 0 \text{ for all } i = 1, 2, \ldots, N.$$

By (5), we establish the existence of a positive constant $D > 0$ such that

$$\begin{aligned}(1-\sigma_n^i)\eta_n^i(1-\mu_n^i)\mu_n^i\|d_n - J_i d_n\|^2 &\leq \|d_n - x^*\|^2 - \|a_n^i - x^*\|^2 \\ &\quad - \sigma_n^i(1-\mu_n^i)\mu_n^i\|d_n - J_i d_n\|^2 \\ &\leq D(\|d_n - x^*\| - \|a_n^i - x^*\|) \\ &\leq D\|d_n - a_n^i\|.\end{aligned}$$

This concludes the proof, as we have shown that

$$\lim_{n\to\infty} \|d_n - J_i d_n\| = 0 \tag{9}$$

for all $i = 1, 2, \ldots, N$.

Applying designated modifications, we procure the ensuing lemmas, which are requisite for the proof of a subsequent theorem.

**Lemma 6.** *Assume that for all $i = 1, 2, \ldots, N$, the following conditions are met:*

*(i)* $\sum_{n=1}^{\infty} |\beta_n|\|x_n - x_{n-1}\| < \infty$;

*(ii)* $(d_n, x^*), (c_n^i, d_n)$ *and* $(b_n^i, d_n) \in E(G)$ *for all* $x^* \in \mathrm{F}$;

*(iii)* $0 < \liminf_{n\to\infty} \mu_n^i \leq \limsup_{n\to\infty} \mu_n^i < 1$;

*(iv)* $\liminf_{n\to\infty} \eta_n^i > 0$ *and* $\limsup_{n\to\infty} \sigma_n^i < 1$.

*Then,* $\lim_{n\to\infty} \|d_n - J_i d_n\| = 0$ *for all* $i = 1, 2, \ldots, N$.

*Proof.* Conditions (ii) and (iv) of Lemma 5 can be replaced by condition (ii) of Lemma 6, and the proof remains valid.

**Lemma 7.** *Assume that for all $i = 1, 2, \ldots, N$, the following conditions are met:*

*(i)* $\sum_{n=1}^{\infty} |\beta_n|\|x_n - x_{n-1}\| < \infty$;

*(ii)* $(x^*, d_n), (d_n, c_n^i)$ *and* $(d_n, b_n^i) \in E(G)$ *for all* $x^* \in \mathrm{F}$;

*(iii)* $0 < \liminf_{n\to\infty} \mu_n^i \leq \limsup_{n\to\infty} \mu_n^i < 1$;

*(iv) either* $\liminf_{n\to\infty} \sigma_n^i > 0$ *or* $\liminf_{n\to\infty} \eta_n^i > 0$ *and* $\limsup_{n\to\infty} \sigma_n^i < 1$.

*Then,* $\lim_{n\to\infty} \|d_n - J_i d_n\| = 0$ *for all* $i = 1, 2, \ldots, N$.

*Proof.* The proof of Lemma 5 remains valid when its conditions (ii), (iv) and (v) are substituted with conditions (ii) and (iv) from Lemma 7.

Building upon the preceding lemmas, we are now ready to present our main result, which establishes the convergence of our proposed algorithm.

**Theorem 1.** *Suppose the following hold.*

*(i) All the conditions in Lemma 3 are satisfied.*

*(ii)* $(d_{n_k}, u) \in E(G)$ *for all* $k$ *whenever* $\{d_{n_k}\}$ *is a subsequence of* $\{d_n\}$ *such that* $d_{n_k} \rightharpoonup u$ *for some* $u \in X$.

*Then, the sequence* $\{x_n\}$ *is weakly convergent in* F.

*Proof.* From Lemmas 2 and 3, $\{\|x_n - x^*\|\}$ converges for all $x^* \in \mathrm{F}$ and $\lim_{n\to\infty} \|d_n - J_i d_n\| = 0$ for all $i = 1, 2, \ldots, N$. Now, let $u$ be a weak sequential cluster point of $\{x_n\}$. It follows that there exists a subsequence $\{x_{n_k}\}$ such that $x_{n_k} \rightharpoonup u$. From condition $(i)$, we have that

$$\|d_n - x_n\| = \|x_n + \beta_n(x_n - x_{n-1}) - x_n\| = |\beta_n|\|x_n - x_{n-1}\|.$$

Taking $n \to \infty$, we have that $\{\|d_n - x_n\|\}$ converges to 0.

This means that $d_{n_k} \rightharpoonup u$. Then, assumption $(ii)$ implies that $(d_{n_k}, u) \in E(G)$. Applying Observation 2, we have that $u \in \mathrm{F}$. Finally, by Observation 1, the sequence $\{x_n\}$ is weakly convergent in F.

The following results are obtained through the application of the previously established lemmas.

**Theorem 2.** *Under the hypotheses of either one of Lemma 4, Lemma 5, Lemma 6 or Lemma 7, and condition* $(ii)$ *of Theorem 1, the sequence* $\{x_n\}$ *is weakly convergent in* F.

*Proof.* The proof is a direct adaptation of that of Theorem 1, originally relying on the conditions in Lemma 3, which equally be substituted with those in Lemma 4, Lemma 5, Lemma 6, or Lemma 7.

We conclude this section with a special case. Observe that nonexpansive mappings are a special case of $G$-nonexpansive mappings when the edge set $E(G)$ contains all possible ordered pairs $(x, y)$ for $x, y \in X$. Indeed, in this case, the condition "for all $x, y \in X$ such that $(x, y) \in E(G)$" simply reduces to "for all $x, y \in X$." This yields the following result.

**Theorem 3.** *For each* $i = 1, 2, \ldots, N$, *let the mapping* $J_i : X \to X$ *be* $G$*-nonexpansive. Assume the following conditions hold:*

*(i)* $\sum_{n=1}^{\infty} |\beta_n| \|x_n - x_{n-1}\| < \infty$;

*(ii)* $0 < \liminf_{n\to\infty} \mu_n^i \leq \limsup_{n\to\infty} \mu_n^i < 1$;

*(iii)* *either* $\liminf_{n\to\infty} \sigma_n^i > 0$ *or* $\liminf_{n\to\infty} \eta_n^i > 0$ *and* $\limsup_{n\to\infty} \sigma_n^i < 1$.

*Then, the sequence* $\{x_n\}$ *is weakly convergent in* F.

*Proof.* It is clear that condition (ii) of Lemma 7 and condition (ii) of Theorem 1 hold. Therefore, by Theorem 2, the sequence $\{x_n\}$ weakly converges to an element in $F$.

## 4. The algorithms proposed for the experimental study

The experimental investigation detailed in the subsequent section aims to assess the performance characteristics of three algorithms. The first algorithm is derived from Algorithm 1 through the imposition of the constraints $\sigma_n^i = 0$ and $\eta_n^i = 1$ for all iterations $n$. For convenience, we will also denote this modification of Algorithm 1 by Algorithm 1 itself.

To facilitate a comprehensive comparative analysis, the study will also incorporate algorithms previously published in the literature, specifically Algorithm 2 and Algorithm 3 presented in [3] and [4], respectively.

**Algorithm 2** [3]

**Initialization:** Choose $x_0, x_1 \in X$, and let $n := 1$.
**Iterative Steps:** Iteratively construct the sequence $\{x_n\}$ as follows.
**Step 1.** Calculate

$$d_n = x_n + \beta_n(x_n - x_{n-1}),$$

where $\{\beta_n\} \subset [0, 1]$.
**Step 2.** Calculate

$$c_n^i = (1 - \mu_n^i)d_n + \mu_n^i J_i d_n \text{ and}$$
$$a_n^i = (1 - \eta_n^i)J_i d_n + \eta_n^i J_i c_n^i,$$

where $\{\mu_n^i\}, \{\eta_n^i\} \subset [0, 1]$ for all $i = 1, 2, \ldots, N$.
**Step 3.** Set

$$x_{n+1} = \arg \max_{1\leq i\leq N} \|a_n^i - d_n\|.$$

Then, proceed by updating $n$ to $n + 1$ and repeating all steps.

**Algorithm 3** [4]

**Initialization:** Choose $x_0, x_1 \in X$, and let $n := 1$.
**Iterative Steps:** Iteratively construct the sequence $\{x_n\}$ as follows.
**Step 1.** Calculate

$$d_n = x_n + \beta_n(x_n - x_{n-1}),$$

where $\{\beta_n\} \subset [0, 1]$.
**Step 2.** Calculate

$$\begin{aligned} c_n^i &= (1 - \mu_n^i)d_n + \mu_n^i J_i d_n, \\ b_n^i &= (1 - \eta_n^i)c_n^i + \eta_n^i J_i c_n^i \text{ and} \\ a_n^i &= (1 - \sigma_n^i)b_n^i + \sigma_n^i J_i b_n^i, \end{aligned}$$

where $\{\mu_n^i\}, \{\eta_n^i\}, \{\sigma_n^i\} \subset [0, 1]$ for all $i = 1, 2, \ldots, N$.
**Step 3.** Set

$$x_{n+1} = \arg \max_{1 \le i \le N} \|a_n^i - d_n\|.$$

Then, proceed by updating $n$ to $n + 1$ and repeating all steps.

## 5. Image recovery problem subject to various types of blur

The process of recovering images degraded by various blurring filters demands a precise mathematical representation. The following equation effectively models this complex scenario, enabling efficient and accurate recovery solutions.

$$h_i = \mathcal{M}_i x^* + \varepsilon_i,$$

where $h_i$ is the observed image that has been blurred by the $i$-th blurring filter, $\mathcal{M}_i$ is the matrix that models the blurring effect for the $i$-th filter, and $\varepsilon_i$ represents the noise present in the observed image $h_i$ for all $i = 1, 2, \ldots, N$.

The objective is to reconstruct the latent image $x^*$ from degraded observations $h_i$, which are corrupted by both blur and noise. This inverse problem is addressed through a sequence of optimization procedures, each corresponding to a different blurring filter:

$$\min_x \quad \zeta_i \|x\|_1 \; + \; \frac{1}{2}\|\mathcal{M}_i x - h_i\|_2^2$$

where $\zeta_i > 0$ is a regularization parameter for all $i = 1, 2, \ldots, N$. To apply our main result in solving the optimization problems, for all $i = 1, 2, \ldots, N$, we define

$$J_i(\cdot) = \text{prox}_{s_i G_i}(I - s_i \nabla F_i)(\cdot),$$

where $F_i(\cdot) = \frac{1}{2}\|\mathcal{M}_i(\cdot) - h_i\|_2^2$, $G_i(\cdot) = \zeta_i \|\cdot\|_1$ and $0 < s_i < \frac{2}{\|\mathcal{M}_i\|_2^2}$. Consequently, $\{J_i : i = 1, 2, \ldots, N\}$ is established as a family of $G$-nonexpansive mappings, given that the associated graph $G$ is the trivially defined complete graph.

(a) Chiang Mai International Airport (CNX) in April 2024

(b) Hazy Skies in Chiang Mai

Figure 1: Original test images.

Figure 1 shows the original test images: (a) Chiang Mai International Airport, with a resolution of $962 \times 1000 \times 3$ pixels, taken with Samsung Galaxy S22 Ultra, and (b) Hazy Skies in Chiang Mai, with a resolution of $1000 \times 862 \times 3$ pixels, selected from the NASA Visible Earth website.

The three blurring filters, $\mathcal{M}_1$, $\mathcal{M}_2$ and $\mathcal{M}_3$, are generated using a motion blur kernel with a motion length of 29. Specifically, $\mathcal{M}_1$ corresponds to an angle of $0°$, $\mathcal{M}_2$ to $45°$, and $\mathcal{M}_3$ to $90°$. An additive zero-mean white Gaussian noise with a standard deviation of $10^{-3}$ is then added for all $i = 1, 2, 3$. The resulting degraded images are presented in Figure 2.

We investigate the behavior of our algorithm and then compare it with Algorithm 2 and Algorithm 3 under the following assumptions.

(i) For recovering Figure 2 (a) - (c), let $x_0 = x_1 = 1 \in X := \mathbb{R}^{962\times1000\times3}$.

(ii) For recovering Figure 2 (d) - (f), let $x_0 = x_1 = 1 \in X := \mathbb{R}^{1000\times862\times3}$.

(iii) Set $\zeta_i = 10^{-3}$, for all $i = 1, 2, 3$.

(iv) Set $t_0 = 1$, and define $t_n = \dfrac{1 + \sqrt{1 + 4t_{n-1}^2}}{2}$ for all $n \in \mathbb{N}$.

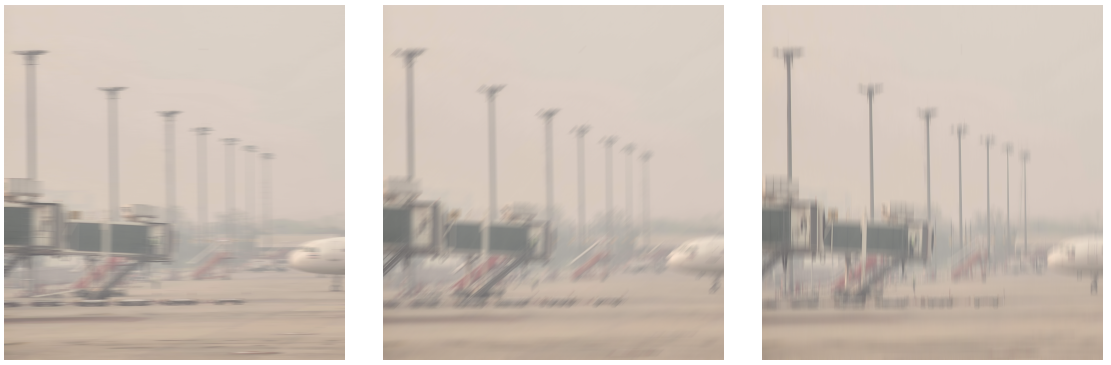

(a) $\mathcal{M}_1$ (b) $\mathcal{M}_2$ (c) $\mathcal{M}_3$

(d) $\mathcal{M}_1$ (e) $\mathcal{M}_2$ (f) $\mathcal{M}_3$

Figure 2: Degraded images.

(v) Define the sequence $\{\beta_n\}$ by

$$\beta_n = \begin{cases} \min\left\{\dfrac{1}{n^2\|x_n - x_{n-1}\|_2}, 0.5\right\} & \text{if } x_n \neq x_{n-1} \text{ and } n > 100; \\ 0.5 & \text{if } x_n = x_{n-1} \text{ and } n > 100; \\ \dfrac{t_{n-1}-1}{t_n} & \text{otherwise} \end{cases}$$

for all $n \in \mathbb{N}$.

The further control parameters of the three algorithms are detailed in Table 1.

Figure 3 (a) - (c) presents the recovered images from Figure 2 (a) - (c) utilizing Algorithm 2, Algorithm 3 and Algorithm 1, respectively. Similarly, Figure 3 (d) - (f) depicts the recovered images from Figure 2 (d) - (f) using the same respective methods. Each image shown in Figure 3 is the result of 100 iterations ($n = 100$). The performance of the algorithms in the image recovery process is quantitatively assessed using Gradient Magnitude Similarity Deviation (GMSD) [20] and Multi-Scale Gradient Magnitude Similarity Deviation (MS-GMSD) [21]. Lower values of GMSD and MS-GMSD indicate greater similarity between the restored and original images, reflecting improved image quality. The GMSD and MS-GMSD values for the recovered images in Figure 3 are presented in Table

2. GMSD and MS-GMSD convergence data for the iterative reconstruction of Figure 2 are presented in Figures 4 and 5.

Table 1: The control parameters of the three algorithms.

| | $s_i$ | $\mu_n^i$ | $\eta_n^i$ | $\sigma_n^i$ |
|---|---|---|---|---|
| Algorithm 2 | $\|\mathcal{M}_i\|_2^{-2}$ | 0.5 | 0.5 | - |
| Algorithm 3 | $\|\mathcal{M}_i\|_2^{-2}$ | 0.5 | 0.5 | 0.5 |
| Algorithm 1 | $\|\mathcal{M}_i\|_2^{-2}$ | 0.5 | 1 | 0 |

Table 2: Performance metrics (GMSD and MS-GMSD) for the recovered images from Figure 3.

| Restored images | GMSD | MS-GMSD |
|---|---|---|
| Fig 3 (a) Algorithm 2 | 0.0039 | 0.0036 |
| Fig 3 (b) Algorithm 3 | 0.0033 | 0.0033 |
| Fig 3 (c) Algorithm 1 | 0.0025 | 0.0030 |
| Fig 3 (d) Algorithm 2 | 0.0249 | 0.0210 |
| Fig 3 (e) Algorithm 3 | 0.0207 | 0.0179 |
| Fig 3 (f) Algorithm 1 | 0.0119 | 0.0115 |

In this experiment, we conduct a numerical comparison of our proposed Algorithm 1 against two existing methods: Algorithm 2 [3] and Algorithm 3 [4]. We evaluate the convergence and reconstruction accuracy of these algorithms using the GMSD and MS-GMSD metrics. Table 2 presents the GMSD and MS-GMSD values for the recovered images shown in Figure 3, offering a quantitative assessment of the performance of three different algorithms. Figures 4 and 5 illustrate the performance of each algorithm, displaying the GMSD and MS-GMSD values as a function of iteration count for the reconstruction of Figure 2.

Table 2 reveals that Algorithm 1 generally achieves the lowest GMSD and MS-GMSD values, indicating better image restoration quality compared to Algorithms 2 and 3, particularly evident in the results for Figure 3 (c) and (f). While Algorithm 3 demonstrates comparable performance in Figure 3 (b) and (e), Algorithm 2 consistently exhibits the highest GMSD and MS-GMSD values across the dataset, suggesting a relatively lower restoration efficacy. The lower values for both metrics in Algorithm 1 suggest that it is more effective in preserving image details and structural similarity after the restoration process.

As seen in Figures 4(a) and 5(a), all three algorithms demonstrate a decreasing trend in GMSD with increasing iterations, indicating convergence toward a solution. However, Algorithm 1 consistently exhibits the lowest GMSD values across all iterations, suggesting better reconstruction accuracy compared to Algorithm 2 and Algorithm 3. In Figure 4,

(a) Algorithm 2 (GMSD = 0.0039 and MS-GMSD = 0.0036)

(b) Algorithm 3 (GMSD = 0.0033 and MS-GMSD = 0.0033)

(c) Algorithm 1 (GMSD = 0.0025 and MS-GMSD = 0.0030)

(d) Algorithm 2 (GMSD = 0.0249 and MS-GMSD = 0.0210)

(e) Algorithm 3 (GMSD = 0.0207 and MS-GMSD = 0.0179)

(f) Algorithm 1 (GMSD = 0.0119 and MS-GMSD = 0.0115)

Figure 3: Results of image recovery as performed by the three algorithms.

Algorithm 1 begins with a GMSD value around 0.25, rapidly reducing the error within the first 15 iterations, then continuing to converge more gradually, ultimately finishing below 0.05 and maintaining the lowest error throughout. In Figure 5, it again shows a sharp reduction in error during the first 20 iterations and continues to outperform the other algorithms. Its MS-GMSD values also remain the lowest across all iterations. This trend is further corroborated by the MS-GMSD analysis in Figures 4(b) and 5(b), where Algorithm 1 again achieves the lowest values. The consistent patterns observed in both GMSD and MS-GMSD metrics confirm the effectiveness of Algorithm 1 in minimizing reconstruction errors.

Algorithm 1 resulted in the lowest GMSD and MS-GMSD values when compared to Algorithm 2 and Algorithm 3, indicating its effectiveness in reconstructing the data represented in Figure 2. While Algorithm 2 and Algorithm 3 also demonstrated convergence, Algorithm 3 generally yielded slightly lower GMSD and MS-GMSD values compared to Algorithm 2. The evidence presented suggests that Algorithm 1 emerges as the preferred

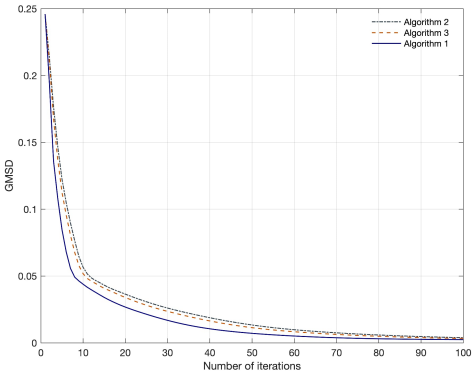


(a) GMSD

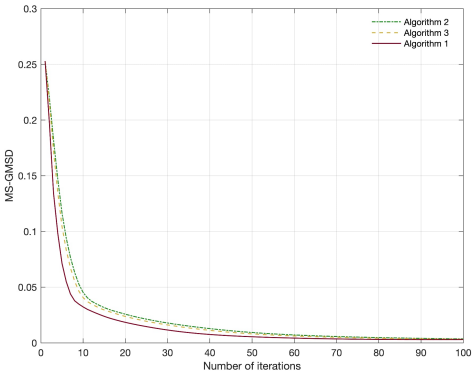


(b) MS-GMSD

Figure 4: GMSD and MS-GMSD values by recovering Figure 2 (a) - (c).

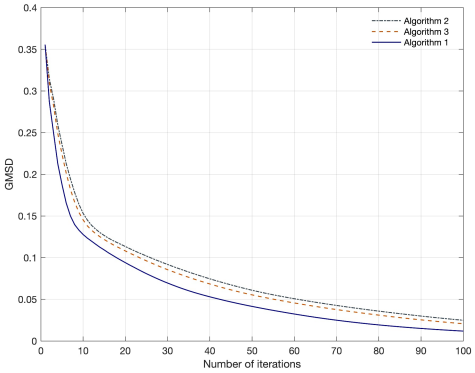


(a) GMSD

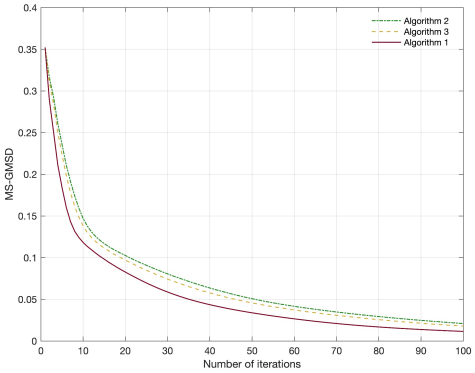


(b) MS-GMSD

Figure 5: GMSD and MS-GMSD values by recovering Figure 2 (d) - (f).

choice for the iterative reconstruction of Figure 2 data, due to its performance in minimizing both metrics. This outcome highlights the importance of selecting an appropriate algorithm to achieve optimal reconstruction accuracy.

## 6. Conclusions

We have presented an algorithm for common fixed point approximation of graph-based mappings in Hilbert spaces and proven its convergence. Its effectiveness in PM2.5-related image recovery was demonstrated and confirmed through comparative analysis, showing competitive performance and higher-quality results. The algorithm's efficiency highlights its ability to optimize computational resources. Furthermore, the convergence behavior directly influences the quality of the numerical results.

Moreover, it is worth noting that the subsequent list of potential reductions indicates Algorithm 1, when simplified, might be reducible to algorithms already established in the literature.

(A) Set $\sigma_n^i = 1$ for all $n \in \mathbb{N}$ and $i = 1, 2, \ldots, N$ in Algorithm 1.

(B) Set $\eta_n^i = 1$ for all $n \in \mathbb{N}$ and $i = 1, 2, \ldots, N$ in Algorithm 1.

(C) Set $\eta_n^i = 0$ for all $n \in \mathbb{N}$ and $i = 1, 2, \ldots, N$ in Algorithm 1.

(D) Set $\sigma_n^i = 0$ for all $n \in \mathbb{N}$ and $i = 1, 2, \ldots, N$ in Algorithm 1.

## Acknowledgements

This research project was supported by:

(i) Fundamental Fund 2025, Chiang Mai University, Chiang Mai, Thailand;

(ii) Thailand Science Research and Innovation (TSRI) (FRB680102/0162);

(iii) Chiang Mai University, Chiang Mai, Thailand;

(iv) Centre of Excellence in Mathematics, MHESI, Bangkok, Thailand.

## References

[1] J. Jachymski. The contraction principle for mappings on a metric space with a graph. *Proceedings of the American Mathematical Society*, 136(4):1359–1373, 2008.

[2] A. Khemphet, R. Suparatulatorn, P. Varnakovida, and P. Charoensawan. A modified parallel algorithm for a common fixed-point problem with application to signal recovery. *Symmetry*, 15(1464), 2023.

[3] N. Jun-On, R. Suparatulatorn, M. Gamal, and W. Cholamjiak. An inertial parallel algorithm for a finite family of G-nonexpansive mappings applied to signal recovery. *AIMS Mathematics*, 7(2):1775–1790, 2022.

[4] D. Yambangwai and T. Thianwan. A parallel inertial SP-iteration monotone hybrid algorithm for a finite family of G-nonexpansive mappings and its application in linear system, differential, and signal recovery problems. *Carpathian Journal of Mathematics*, 40(2):535–557, 2024.

[5] R. Suparatulatorn, P. Saksuriya, T. Suebcharoen, and K. Chaichana. An iterative approach to common fixed points of G-nonexpansive mappings with applications in solving the heat equation. *Axioms*, 13(11):729, 2024.

[6] P. Sridarat, R. Suparatulatorn, S. Suantai, and Y. J. Cho. Convergence analysis of SP-iteration for G-nonexpansive mappings with directed graphs. *Bulletin of the Malaysian Mathematical Sciences Society*, 42(5):2361–2380, 2019.

[7] S. Suantai, M. Donganont, and W. Cholamjiak. Hybrid methods for a countable family of G-nonexpansive mappings in hilbert spaces endowed with graphs. *Mathematics*, 7(10):936, 2019.

[8] S. Suantai, K. Kankam, P. Cholamjiak, and W. Cholamjiak. A parallel monotone hybrid algorithm for a finite family of G-nonexpansive mappings in hilbert spaces endowed with a graph applicable in signal recovery. *Computational and Applied Mathematics*, 40(4):145, 2021.

[9] P. Charoensawan, D. Yambangwai, W. Cholamjiak, and R. Suparatulatorn. An inertial parallel algorithm for a finite family of G-nonexpansive mappings with application to the diffusion problem. *Advances in Difference Equations*, 2021(453), 2021.

[10] J. J. Liaw, Y. F. Huang, C. H. Hsieh, D. C. Lin, and C. H. Luo. PM2.5 concentration estimation based on image processing schemes and simple linear regression. *Sensors*, 20(8):2423, 2020.

[11] J. Ma, K. Li, Y. Han, P. Du, and J. Yang. Image-based PM2.5 estimation and its application on depth estimation. In *2018 IEEE International Conference on Acoustics, Speech and Signal Processing (ICASSP)*, pages 1857–1861, Calgary, AB, Canada, 2018.

[12] T. Zheng, M. H. Bergin, S. Hu, J. Miller, and D. E. Carlson. Estimating ground-level PM2.5 using micro-satellite images by a convolutional neural network and random forest approach. *Atmospheric Environment*, 230:117451, 2020.

[13] K. Gu, J. Qiao, and X. Li. Highly efficient picture-based prediction of PM2.5 concentration. *IEEE Transactions on Industrial Electronics*, 66(4):3176–3184, 2019.

[14] H. Wang, X. Yuan, X. Wang, Y. Zhang, and Q. Dai. Real-time air quality estimation based on color image processing. In *2014 IEEE Visual Communications and Image Processing Conference*, pages 326–329, Valletta, Malta, 2014.

[15] M. Abbas and T. Nazir. A new faster iteration process applied to constrained minimization and feasibility problems. *Matematički Vesnik*, 66(3):223–234, 2014.

[16] M. R. Alfuraidan and M. A. Khamsi. Fixed points of monotone nonexpansive mappings on a hyperbolic metric space with a graph. *Fixed Point Theory and Applications*, 2015(1):44, 2015.

[17] H. H. Bauschke and P. L. Combettes. *Convex analysis and monotone operator theory in Hilbert spaces*. CMS Books in Mathematics. Springer, New York, NY, USA, 2011.

[18] A. Auslender, M. Teboulle, and S. Ben-Tiba. A logarithmic-quadratic proximal method for variational inequalities. *Computational Optimization and Applications*, 12(1):31–40, 1999.

[19] R. Suparatulatorn, S. Suantai, and W. Cholamjiak. Hybrid methods for a finite family of G-nonexpansive mappings in hilbert spaces endowed with graphs. *AKCE International Journal of Graphs and Combinatorics*, 14(2):101–111, 2017.

[20] W. Xue, L. Zhang, X. Mou, and A. C. Bovik. Gradient magnitude similarity deviation: A highly efficient perceptual image quality index. *IEEE Transactions on Image Processing*, 23(2):684–695, 2014.

[21] B. Zhang, P. V. Sander, and A. Bermak. Gradient magnitude similarity deviation on multiple scales for color image quality assessment. In *2017 IEEE International*

*Conference on Acoustics, Speech and Signal Processing (ICASSP)*, pages 1253–1257, New Orleans, LA, USA, 2017.